Studies in Applied Mathematics

WILEY

STUDIES IN APPLIED MATHEMATICS

ORIGINAL ARTICLE OPEN ACCESS

Thermal Convection in a Linearly Viscous Fluid Overlying a Bidisperse Porous Medium

P. Dondl[1] | B. Straughan[2]

[1]Abteilung für Angewandte Mathematik, Albert-Ludwigs-Universität Freiburg, Freiburg, Germany | [2]Department of Mathematics, University of Durham, Durham, UK

Correspondence: P. Dondl (patrick.dondl@mathematik.uni-freiburg.de)

Received: 13 May 2024 | **Revised:** 24 October 2024 | **Accepted:** 18 November 2024

Funding: The work was supported by an Emeritus Fellowship of the Leverhulme Trust (EM-2019-022/9).

Keywords: bidisperse porous–viscous fluid layer | bimodal | Chebyshev tau method | instability | thermal convection

ABSTRACT

A bidisperse porous medium is one with two porosity scales. There are the usual pores known as macropores but also cracks or fissures in the skeleton which give rise to micropores. In this article, we develop and analyze a model for thermal convection where a layer of viscous incompressible fluid overlies a layer of bidisperse porous medium. Care has to be taken with the boundary conditions at the interface of the fluid and the porous material, and this aspect is investigated. We propose two Beavers–Joseph conditions at the interface and we argue that the parameters in these relations should be different since they depend on the macro or micro permeability, and these parameters are estimated from the original experiments of Beavers and Joseph. The situation is one in a layer which is heated from below and under appropriate conditions bimodal neutral curves are found. These can depend on the relative permeability between the macro and micropores, the Beavers–Joseph conditions appropriate to the macro or micropores, the ratio $\hat{d}$ of the depth d of the fluid layer to the depth d_m of the porous layer, or generally the nature of the bidisperse medium.

1 | Introduction

The problem of flow of a fluid overlying a porous medium saturated by the same fluid is one which has attracted the attention of many prominent scientists. A fundamental interface condition between the fluid and the porous medium was proposed by Beavers and Joseph [4]. The first analysis of thermal convection in the situation where a fluid overlies a saturated porous medium is due to Nield [44] who successfully employed the Beavers–Joseph boundary condition to derive a satisfactory model. A surprising result for the same thermal convection problem was discovered by Chen and Chen [16] who showed that the ratio of fluid depth, d, to porous layer depth, d_m, defined by $\hat{d} = d/d_m$, is critical to determining the process for the onset of thermal convection in the two-layer system. If $\hat{d}$ is below a critical value then convection commences in the porous layer whereas when $\hat{d}$ is above the critical value then convection commences in the fluid. This class of problem was further investigated both experimentally and theoretically by Chen and Chen [17, 18], Chen [15], McKay and Straughan [41], where the last mentioned article applies the theory to the problem of stone formation into regular patterns at the bottom of a shallow lake.

The subject of thermal convection or generally flow in a two-layer system has been studied in much detail with a review of the early work and applications to various areas in industry or geophysics given in chapter 6 of Straughan [58]. The intense interest in this class of problem has been driven by the many applications to diverse areas such as heat pipe technology, renewable energy, and desalination (see, e.g., Kumaravel, Nagaraj, and Barmavatu

[35], Straughan [58]), contaminant dispersal in water ways (Hibi and Tomigashi [28], Hibi [27]), or even blood flow in arteries and veins in the human body (see, e.g., Sharma and Yadav [55], Tiwari, Shah, and Chauhan [63], Ponalagusamy and Manchi [48], Wajihah and Sankar [65]). Indeed, the last mentioned article involves five-layer flow comprising Darcy media, Brinkman media, plasma, core flow, and plug flow.

There are many recent stability analyses of fluid flow in the two-layer fluid–porous configuration (see, e.g., Anjali, Khan, and Bera [1], Barman, Aleria, and Bera [3], Carr and Straughan [10], Chang, Chen, and Straughan [13], Hill and Straughan [29, 31], Hooshyar, Yoshikawa, and Mirbod [33], Mirbod et al. [42], Chang, Chen, and Chang [14], Samanta [51–53], Wu and Mirbod [68], Yin, Wang, and Wang [69], and Tsiberkin [64]). Particular analyses involving the nonlinear theory and bifurcations are given by Han, Wang, and Wang [26], McCurdy, Moore, and Wang [40], Lyu and Wang [39], and Hill and Straughan [30]. In addition, mathematical analysis of the structural stability of the two-layer system has been thoroughly investigated (see, e.g., Li, Xiao, and Lin [36], Li, Zhang, and Zin [38], Li, Chen, and Shi [37], and Payne and Straughan [47].

In a separate development, there has been immense interest in thermal convection in a single layer of saturated porous material but when the porous skeleton is of double porosity type. By double porosity, we mean that the solid skeleton contains pores of a visible size known as macropores, but the skeleton itself contains cracks or fissures which give rise to much smaller micropores. Flow in such materials is additionally called bidisperse or bidispersive. The thermal convection problem in a bidisperse porous material was first developed by Nield and Kuznetsov [46] who allowed for different velocities, pressures, and temperature fields in the macro and microphases and a critical review of the topic is given by Gentile and Straughan [25]. There are many recent contributions driven by the need to understand bidispersive convection in real-life applications (cf. Gentile and Straughan [25], Straughan [59, chapter 13]). Analyses of bidispersive thermal convection in isotropic, anisotropic, vertical layer, inclined layer, and with rotation effects are given by Badday and Harfash [2], Capone, De Luca, and Gentile [7, 8], Capone and De Luca [5], Capone and Massa [6], Capone, De Luca, and Massa [9], Chaloob, Harfash, and Harfash [11], Falsaperla, Mulone, and Straughan [21], Gentile and Straughan [23, 24], Saravanan and Vigneshwaran [54], Straughan [60–62], and the structural stability aspect of the system of equations is considered by Franchi, Nibbi, and Straughan [22].

The object of the current work is to present a model for thermal convection in an incompressible viscous fluid when that fluid overlies a bidispersive porous medium saturated with the same fluid. We analyze the instability of thermal convection in this system and show that while there are definite relations between the onset of convective motion and the respective depths of the fluid and porous layers, the properties of the bidisperse porous medium strongly affect when convection will arise and whether it initiates in the porous or fluid layer. The relative permeability of the macro to the micropores plays a key role in the convection process. We also propose two Beavers–Joseph interface conditions and the parameters in these relations play a major role. This is the first analysis we have seen of this problem, and we believe it has much future application in diverse areas such as blood flow, heat transfer, and renewable energy.

2 | Basic Equations

We suppose a linearly viscous incompressible fluid is contained in the infinite layer $\mathbb{R}^2 \times \{0 < z < d\}$ and below this is a bidisperse porous medium saturated with the same fluid and this occupies the infinite layer $\mathbb{R}^2 \times \{-d_m < z < 0\}$, with gravity acting in the negative z-direction.

The equations for the fluid in the layer $\mathbb{R}^2 \times \{0 < z < d\}$ are then (cf. Chandrasekhar [12]),

$$\begin{aligned} &V_{i,t} + V_j V_{i,j} = -\frac{1}{\rho_0} p_{,i} + \nu \Delta V_i + \gamma g k_i T, \\ &V_{i,i} = 0, \\ &T_{,t} + V_i T_{,i} = \frac{k_f}{(\rho_0 c_p)_f} \Delta T, \end{aligned} \tag{1}$$

where $V_i(\mathbf{x}, t)$ is the velocity field, $T(\mathbf{x}, t)$ is the temperature field, $p(\mathbf{x}, t)$ is the pressure field, $\mathbf{x}$ is the spatial point in the layer, and t is time. We use indicial notation throughout in conjunction with the Einstein summation convention, so that, for example,

$$\begin{aligned} V_i T_{,i} \equiv \sum_{i=1}^{3} V_i T_{,i} &\equiv V_1 \frac{\partial T}{\partial x_1} + V_2 \frac{\partial T}{\partial x_2} + V_3 \frac{\partial T}{\partial x_3} \\ &\equiv U \frac{\partial T}{\partial x} + V \frac{\partial T}{\partial y} + W \frac{\partial T}{\partial z}, \end{aligned}$$

where $\mathbf{V} = (V_1, V_2, V_3) \equiv (U, V, W)$. In Equations (1), $\gamma, g, \rho_0, k_f, \nu$, and c_p are the thermal expansion coefficient of the fluid, gravity, reference density, thermal conductivity of the fluid, kinematic viscosity of the fluid, and specific heat at constant pressure of the fluid. The vector $\mathbf{k} = (0, 0, 1)$ and Δ is the Laplacian

$$\Delta = \frac{\partial^2}{\partial x^2} + \frac{\partial^2}{\partial y^2} + \frac{\partial^2}{\partial z^2}.$$

For an isotropic bidisperse porous material, we suppose the macroporosity is ϕ, the microporosity is ϵ. If we denote (U_i^f, p^f) to be the pore averaged velocity and pressure in the macropores and (U_i^p, p^p) to be the pore averaged velocity and pressure in the micropores, then the governing equations of flow in the bidisperse porous medium may be written (cf. Gentile and Straughan [23], Straughan [60])

$$\begin{aligned} &-\frac{\mu}{K_f} U_i^f - \zeta\left(U_i^f - U_i^p\right) - p_{,i}^f + \rho_0 \gamma k_i g T^m = 0, \\ &U_{i,i}^f = 0, \\ &-\frac{\mu}{K_p} U_i^p - \zeta\left(U_i^p - U_i^f\right) - p_{,i}^p + \rho_0 \gamma k_i g T^m = 0, \\ &U_{i,i}^p = 0, \\ &(\rho_0 c)_m T_{,t}^m + (\rho_0 c)_f \left(U_i^f + U_i^p\right) T_{,i}^m = k_m \Delta T^m, \end{aligned} \tag{2}$$

where $T^m(\mathbf{x}, t)$ is the temperature field of the fluid in the bidisperse porous medium.

Equations (1) hold on the domain $\{(x, y) \in \mathbb{R}^2\} \times \{z \in (0, d)\} \times \{t > 0\}$ while (2) hold on the domain $\{(x, y) \in \mathbb{R}^2\} \times \{z \in (-d_m, 0)\} \times \{t > 0\}$. Equations (2) assume Darcy's law holds and a Boussinesq approximation is employed. The variable μ is the dynamic viscosity of the fluid, K_f and K_p are the macro and micro permeabilities, ζ is an interaction coefficient which represents the momentum transfer between the macro and microphases, and $(\rho_0 c)_m$, k_m are given by

$$(\rho_0 c)_m = (1-\phi)(1-\epsilon)(\rho_0 c)_s + \phi(\rho_0 c)_f + \epsilon(1-\phi)(\rho_0 c)_p\,,$$

and

$$k_m = (1-\phi)(1-\epsilon)k_s + \phi k_f + \epsilon(1-\phi)k_p\,,$$

where s, f, and p denote values in the solid skeleton, the fluid in the macropores, and the fluid in the micropores.

The boundary conditions at the top and bottom of the layer, $z = d$ and $z = -d_m$ are specified as follows:

$$\begin{aligned} &V_i = 0, \quad T = T_U, \qquad \text{on } z = d,\\ &U_3^f = 0, \quad U_3^p = 0, \quad T^m = T_L, \qquad \text{on } z = -d_m\,, \end{aligned} \tag{3}$$

where T_U, T_L are constants with $T_L > T_U > 0$. Under these conditions, (1) and (2) admit a steady conduction solution of form

$$\begin{aligned} &\bar{U}_i^f = 0, \qquad \bar{U}_i^p = 0, \qquad \bar{V}_i = 0,\\ &\bar{T} = T_0 - (T_0 - T_U)\frac{z}{d}\,, \qquad 0 \le z \le d,\\ &\bar{T}^m = T_0 - (T_L - T_0)\frac{z}{d_m}\,, \qquad -d_m \le z \le 0, \end{aligned} \tag{4}$$

where we have employed the fact that the temperature is continuous across the interface $z = 0$. To determine the constant T_0, we require the heat flux to be continuous across the interface $z = 0$ and then

$$k_m \frac{d\bar{T}^m}{dz} = k_f \frac{d\bar{T}}{dz}\,, \qquad \text{at } z = 0.$$

This yields T_0 as

$$T_0 = \frac{k_f T_U d_m + k_m T_L d}{d k_m + d_m k_f}\,. \tag{5}$$

The initial conditions required for the evolution problem are the prescription of the initial values of V_i, T, T^m, that is, prescription of $V_i(\mathbf{x}, 0), T(\mathbf{x}, 0)$, and $T^m(\mathbf{x}, 0)$.

3 | Perturbation Equations

As our goal is to study instability of the base solution (4), we now introduce perturbations to the variables $V_i, T, p^f, U_i^f, U_i^p, T^m$, and p^p as $u_i, \theta, \pi^f, u_i^f, u_i^p, \theta^m$, and π^p. We derive the perturbation equations for these variables from Equations (1) and (2). However, it is convenient to present these in nondimensional form with length scales d, d_m in the fluid and bidisperse porous layers, and with corresponding velocity scales U and U^m, although we here select $U = U^m$. The time scales are $\mathcal{T}$ and $\mathcal{T}^m$ where $\mathcal{T} = d^2/\nu$, with $\nu = \mu/\rho_0$ and we pick $\mathcal{T} = \mathcal{T}^m$. The pressure scale is $P = \mu U/d$. The temperature scales are

$$T^\sharp = \frac{U(T_0 - T_U)d(\rho_0 c_p)_f}{k_f}$$

and

$$T_m^\sharp = U^m(T_l - T_0)\frac{d_m(\rho_0 c_p)_f}{k_m}$$

and thus one finds

$$\frac{T^\sharp}{T_m^\sharp} = \left(\frac{k_m}{k_f}\right)^2 \hat{d}^2\,, \qquad \frac{T_0 - T_U}{T_L - T_0} = \frac{k_m}{k_f}\,\hat{d},$$

where $\hat{d} = d/d_m$. It is convenient to introduce the notation

$$\hat{k} = \frac{k_f}{k_m}\,, \qquad \hat{\kappa} = \frac{(\rho_0 c)_m}{(\rho_0 c)_f}\,\hat{k}\,,$$

and to define the Prandtl number, Pr, and the porous Prandtl number, Pr_m, by

$$Pr = \frac{\nu}{\kappa} = \frac{\mu}{\rho_0}\frac{(\rho_0 c_p)_f}{k_f}\,, \qquad Pr_m = \frac{\mu}{\rho_0}\frac{(\rho_0 c)_m}{k_m}$$

from which one may show $Pr_m = \hat{\kappa} Pr$.

The fluid and porous Rayleigh numbers Ra and Ra^m are defined by

$$Ra = \frac{\gamma g d^4}{\kappa_f \nu}\frac{(T_0 - T_U)}{d}\,, \tag{6}$$

where $\kappa_f = k_f/(\rho_0 c_p)_f$, and

$$Ra_m = \gamma g K^f \frac{(T_L - T_0)}{d_m}\frac{d_m^2}{[k_m/(\rho_0 c)_f]\nu}\,, \tag{7}$$

from which one shows

$$Ra = \left(\frac{\hat{d}}{\hat{k}}\right)^2 \frac{Ra_m}{Da},$$

where Da is the Darcy number defined here as

$$Da = \frac{K_f}{d^2}\,.$$

The relative permeability K_r is defined by $K_r = K_f/K_p$, and another useful nondimensional variable is $\delta = \sqrt{K_p}/d_m$, from which we may see that $Da = K_r \delta^2/\hat{d}^2$.

With the above nondimensionalization one may show that the linearized fluid perturbation equations have form

$$\begin{aligned} u_{i,t} &= -\pi_{,i} + \Delta u_i + Rak_i\theta, \\ u_{i,i} &= 0, \\ Pr\theta_{,t} &= w + \Delta\theta, \end{aligned} \tag{8}$$

where $w = u_3$ and these equations hold on $\mathbb{R}^2 \times \{z \in (0,1)\} \times \{t > 0\}$ while the linearized bidispersive porous media equations have form

$$\begin{aligned} &-u_i^f - \xi(u_i^f - u_i^p) - \pi_{,i}^f + Ra^m k_i \theta^m = 0, \\ &u_{i,i}^f = 0, \\ &-K_r u_i^p - \xi(u_i^p - u_i^f) - \pi_{,i}^p + Ra^m k_i \theta^m = 0, \\ &u_{i,i}^p = 0, \\ &\frac{Pr^m}{\hat{d}^2}\,\theta_{,t}^m = w^f + w^p + \Delta\theta_m, \end{aligned} \tag{9}$$

where $w^f = u_3^f, w^p = u_3^p$ and Equations (9) hold on $\mathcal{R}^2 \times \{z_m \in (-1,0)\} \times \{t > 0\}$. The nondimensional momentum transfer interaction coefficient ξ is defined by $\xi = \zeta K_f/\mu$.

Equations (8) and (9) when reduced to the thermal convection instability problem essentially represent a 12th-order system of equations. We thus require 12 boundary conditions. In this work, we employ a normal-mode instability analysis and it is sufficient to require the following conditions:

$$w = w' = \theta = 0, \qquad \text{on } z = 1,$$

where $w' = \partial w/\partial z$. This corresponds to a fixed upper surface. Also,

$$w^f = w^p = \theta^m = 0, \qquad \text{on } z = -1.$$

The remaining six boundary conditions come from considerations on the interface $z = 0$. To retain conservation of mass flow across the interface, we require

$$w = w^m,$$

where $w^m = w^f + w^p$. Likewise, the dimensional temperatures are continuous so

$$\theta = \theta_m, \qquad \text{at} \qquad z = 0.$$

In addition, the normal component of heat flux $\mathbf{q} \cdot \mathbf{n}$ is continuous across $z = 0$. Three further conditions are needed and these arise by requiring continuity of normal stress, and by appealing to a combination of appropriate forms of the experimentally verified Beavers and Joseph [4] condition. Details of these boundary conditions are amplified below.

4 | Instability Analysis

The next step is to remove the pressure terms π, π^f, and π^p from (8) and (9), and this we do by taking curl of Equations $(8)_1$ and $(9)_{1,3}$ and retaining the third component. This results in the system of equations

$$\begin{aligned} \sigma\Delta w &= \Delta^2 w + Ra\Delta^*\theta, \\ \sigma Pr\theta &= w + \Delta\theta, \end{aligned} \tag{10}$$

and

$$\begin{aligned} &(1+\xi)\Delta w^f - \xi\Delta w^p - Ra^m\Delta^*\theta^m = 0, \\ &(K_r+\xi)\Delta w^p - \xi\Delta w^f - Ra^m\Delta^*\theta^m = 0, \\ &\frac{\sigma_m Pr_m}{\hat{d}^2}\,\theta^m = w^f + w^p + \Delta\theta^m, \end{aligned} \tag{11}$$

where we have represented time by $e^{\sigma t}$ in the fluid equations and by $\exp(\sigma_m t)$ in the bidispersive porous equations. The symbol Δ^* is the horizontal Laplacian. Equations (10) hold on $\mathbb{R}^2 \times (0,1)$ while (11) hold on $\mathbb{R}^2 \times (-1,0)$.

We next solve $(11)_{1,2}$ in terms of Δw^f and Δw^p. We represent w and θ as $w = W(z)h(x,y)$, $\theta = \Theta(z)h(x,y)$, and $w^f = W^f(z)h^m(x,y)$, $w^p = W^p(z)h^m(x,y)$, $\theta_m = \Theta_m(z)h^m(x,y)$, where h and h_m are plan forms which tile the plane (cf. Chandrasekhar [12], pp. 43–52), and are typical of the hexagonal convection cell forms found in real life. The functions h and h_m satisfy the relations $\Delta^* h = -a^2 h$ and $\Delta^* h_m = -a_m^2 h_m$, for wavenumbers a and a_m. We reduce $(10)_1$ to two second-order equations by setting $\Delta w = \chi$, and then we arrive at the following coupled system of equations to solve for the growth rate (eigenvalues) σ, σ_m:

$$\begin{aligned} &(D^2 - a^2)W - \chi = 0, \\ &(D^2 - a^2)\chi - Ra\,a^2\Theta = \sigma\chi, \\ &(D^2 - a^2)\Theta + W = Pr\,\sigma\,\Theta \end{aligned} \tag{12}$$

on $z \in (0,1)$, where $D = d/dz$, and

$$\begin{aligned} &(D^2 - a_m^2)W^f + Ra_m\,a_m^2\,\frac{(K_r+2\xi)}{(K_r+\xi+\xi K_r)}\,\Theta_m = 0, \\ &(D^2 - a_m^2)W^p + Ra_m\,a_m^2\,\frac{(1+2\xi)}{(K_r+\xi+\xi K_r)}\,\Theta_m = 0, \\ &(D^2 - a_m^2)\Theta_m + W^f + W^p = \frac{Pr_m}{\hat{d}^2}\,\sigma_m\,\Theta_m \end{aligned} \tag{13}$$

on $z_m \in (-1,0)$.

The nondimensional boundary conditions are

$$\begin{aligned} W = W' = \Theta = 0, \qquad z = 1, \\ W^f = W^p = \Theta^m = 0, \qquad z = -1, \end{aligned} \tag{14}$$

together with the nondimensional interface conditions

$$W = W^p + W^f \equiv W^m, \qquad z = 0,$$
$$\theta_m = \theta\left(\frac{k_m}{k_f}\right)^2 \hat{d}^2, \qquad \frac{d\theta_m}{dz_m} = \frac{d\theta}{dz}\,\hat{d}\,\frac{k_m}{k_f}, \qquad z = 0, \tag{15}$$

where the latter two arise due to continuity of temperature, and continuity of heat flux.

Equations (12) and (13) represent a 12th-order eigenvalue problem. We thus require three more conditions on the interface. Many approaches to interface conditions have been suggested in the one-porosity case (see Ehrhardt [20]). In this work, we follow the approach of Beavers and Joseph [4] which was proposed for the one-porosity model and we adapt it to be applicable to the bidisperse situation. Thus, for the remaining interface conditions we argue as follows.

In terms of the fluid and pore averaged velocities at the microscopic level, the Beavers and Joseph [4] condition may be applied separately to the macro and microcomponents to yield in dimensionless form

$$\frac{1}{d}\frac{\partial u_\beta}{\partial z} = \frac{\alpha_f}{\sqrt{K_f}}\left(u_\beta - u_\beta^f\right), \qquad \beta = 1, 2, \tag{16}$$

and

$$\frac{1}{d}\frac{\partial u_\beta}{\partial z} = \frac{\alpha_p}{\sqrt{K_p}}\left(u_\beta - u_\beta^p\right), \qquad \beta = 1, 2, \tag{17}$$

where α_f and α_p are experimentally determined constants. For a single-porosity material, Beavers and Joseph [4] write that "α *is a dimensionless quantity depending on the material parameters which characterize the structure of permeable material within the boundary region.*" Beavers and Joseph [4] estimate the values of α for a one-porosity material by performing an experiment with demineralized water or a specific oil flowing over a foametal block. The blocks were of five types of porous material which they call Foametal A, Foametal B, Foametal C, and two types of aloxite. The permeabilities are all different and vary from 10^{-6}in^2 to $12.7\times10^{-5}\text{in}^2$. The average pore sizes vary from 0.013 to 0.045 in. On the basis of their experimental results, they obtain values of α*in the one-porosity case* of $\alpha = 0.1$ (twice), 0.78, 1.45, and 4.0. If one graphs the Beavers and Joseph [4] values of α against the permeability K then it appears there is a definite increase of α with K. With a bidispersive material, we have different permeabilities K^f and K^p in the macro and micropores. Thus, we believe using the results of Beavers and Joseph [4], we should employ different values of α in each of the two Beavers–Joseph conditions. We denote these by α^f and α^p. In this work, we keep α^p fixed at value $\alpha^p = 0.1$ and then employ values of K_r estimated by Gentile and Straughan [25] for real porous materials. Using these values and that of α^p, we then know K^f and so we may estimate α^f from a graphical representation of Beavers and Joseph [4]. When $K_r = 10$, we estimate α^f to be in the range $0.3 \le \alpha^f \le 0.65$. When $K_r = 25$, we estimate α^f to be in the range $0.6 \le \alpha^f \le 1.25$. We also use $K_r = 151.7$ and this is consistent with a value of $\alpha^f = 4$, although we also compute with $\alpha^f = 2$ in this case.

We differentiate (16) and (17) and employ the incompressibility conditions to derive the interface conditions

$$w_{zz} = A_f w_z - A_f \hat{d} w_{z_m}^f \tag{18}$$

and

$$w_{zz} = A_p w_z - A_p \hat{d} w_{z_m}^p, \tag{19}$$

where the derivatives are with respect to z, z_m nondimensional, $0 \le z \le 1$, $-1 \le z_m \le 0$, and where

$$A_f = \frac{\alpha_f d}{2\sqrt{K_f}}, \qquad A_p = \frac{\alpha_p d}{2\sqrt{K_p}}. \tag{20}$$

For the final interface condition, we argue that continuity of normal stress at the interface $z = 0$ requires

$$\pi^f + \pi^p = \pi - \mu w_z,$$

or in nondimensional form

$$\pi^f + \pi^p = \pi - w_z, \qquad \text{on } z = 0. \tag{21}$$

Equation (21) is differentiated with respect to $x_\eta, \eta = 1, 2$, and one then employs the differential Equations $(8)_{1,2}$ and $(9)_{1-4}$ in the forms

$$\begin{aligned} &\pi_{,\eta} = \Delta u_\eta - \sigma u_\eta, \qquad u_{\eta,\eta} + w_{,z} = 0,\\ &\pi_{,\eta}^f = -u_\eta^f - \xi\left(u_\eta^f - u_\eta^p\right), \qquad u_{\eta,\eta}^f + w_{,z}^f = 0,\\ &\pi_{,\eta}^p = -K_r u_\eta^p - \xi\left(u_\eta^p - u_\eta^f\right), \qquad u_{\eta,\eta}^p + w_{,z}^p = 0 \end{aligned} \tag{22}$$

to eliminate the pressure terms. We differentiate (21) and employ (22) to find

$$\sigma w_{,z} - \Delta w_{,z} - \Delta^* w_{,z} = w_{,z}^f + K_r w_{,z}^p.$$

The differentiated form of (21) is rewritten using (22) as

$$-u_\eta^f - K_r u_\eta^p = \Delta u_\eta - \sigma u_\eta - 2\mu w_{,z\eta}, \tag{23}$$

where $\eta = 1, 2$. Note that in this case the ξ terms disappear. Now differentiate (23) for $\eta = 1$ with respect to x and for $\eta = 2$ with respect to y. This yields after summation to

$$-u_{\eta,\eta}^f - K_r u_{\eta,\eta}^p = \Delta u_{\eta,\eta} - \sigma u_{\eta,\eta} - w_{,z\eta\eta}.$$

Then, use the incompressibility conditions to find

$$w_{,z}^f + K_r w_{,z}^p = -\Delta w_{,z} + \sigma w_{,z} - \Delta^* w_{,z}, \tag{24}$$

where $\Delta^* = \partial^2/\partial x^2 + \partial^2/\partial y^2$. Equation $(22)_3$ allows one to determine the following nondimensional interface condition

$$D_m w^f + KrD_m w^p = \sigma Dw - D\Delta w - \Delta^* Dw, \tag{25}$$

where $D = d/dz, z \in (0, 1), D_m = d/dz_m, z_m \in (-1, 0)$.

Thus, the complete set of boundary conditions are (14), (15), together with (18), (19), and (25).

5 | Numerical Method

We solve Equations (12) and (13) by a Chebyshev tau method (cf. Dongarra, Straughan, and Walker [19]) coupled with the QZ algorithm for a generalized matrix eigenvalue problem (cf. Moler and Stewart [43]). Equations (12) are transformed into the Chebyshev domain $(-1, 1)$ and Equations (13) are likewise transformed into the same domain with the interface now being $z = -1$, with the transformations $z_m = -2\hat{z}_m - 1$, $z = 2\hat{z} - 1$. The variables $W, \chi, \Theta, W^f, W^p$, and Θ^m are written as finite series of Chebyshev polynomials, for example,

$$W = \sum_{i=0}^{N} W_i T_i(z)$$

for Fourier coefficients W_i. This yields a block matrix generalized eigenvalue problem of form $A\mathbf{x} = \sigma B\mathbf{x}$ for $6N \times 6N$ matrices A, B with B singular, where

$$\mathbf{x} = (\tilde{W}, \tilde{\chi}, \tilde{\Theta}, \tilde{W}^f, \tilde{W}^p, \tilde{\Theta}^m),$$

$\tilde{W}$, and so forth, being the truncated versions of W, and so forth, that is,

$$\tilde{W} = (W_0, \dots, W_N), \dots, \tilde{\Theta}^m = (\Theta_0^m, \dots, \Theta_N^m).$$

The boundary conditions are likewise expanded in Chebyshev polynomials and added as rows of the matrices A and B via a similar procedure to that explained in Dongarra, Straughan, and Walker [19].

The complete set of boundary conditions on $z = 1$ or $z = -1$ are now

$$\begin{aligned}
&W = 0,\ DW = 0,\ \Theta = 0,\ W^f = 0,\ W^p = 0,\ \Theta_m = 0, \quad z = 1,\\
&W = W^f + W^p \equiv W^m, \quad z = -1,\\
&\Theta_m = \Theta\,\frac{\hat{d}^2}{\hat{k}^2}, \quad D_m\Theta_m + \frac{\hat{d}}{\hat{k}}\,D\Theta = 0, \quad z = -1,\\
&D\chi - a^2 DW - D_m W^f - K_r D_m W^p = 0, \quad z = -1,\\
&\chi + a^2 W - \frac{\alpha^f}{2}\,DW - \frac{\alpha^f}{2}\,\hat{d}\,D_m W^f = 0, \quad z = -1,\\
&\chi + a^2 W - \frac{\alpha^p}{2}\,DW - \frac{\alpha^p}{2}\,\hat{d}\,D_m W^p = 0, \quad z = -1.
\end{aligned} \tag{26}$$

In our computations, we employed the value of $N = 30$. We varied N and found that once this number is 30 convergence of each variable is achieved. This is typical in convection problems, although it is not the case in other areas such as shear flow.

6 | Numerical Results

This section reports on numerical results for the critical Rayleigh number and critical wavenumber for the equations for thermal convection in a linearly viscous fluid overlying a bidisperse porous material. We choose parameter values appropriate to water being the working fluid and a bidisperse porous material being based upon a glass bead skeleton.

As this is the first calculation for this problem, we base our calculations for α^f and α^p on the results of the experimental work of Beavers and Joseph [4], as explained in Section 4. For numerical values of the many parameters, we refer to Gentile and Straughan [25] who employed tabulated experimental values of Hooman, Sauret, and Dahari [32], Imani and Hooman [34], Chen [15], Rees [49, 50], and Nield [45]. In particular, two key articles pertaining to the bidisperse porous medium theory of Nield and Kuznetsov [46] were presented by Hooman, Sauret, and Dahari [32] and by Imani and Hooman [34]. Hooman, Sauret, and Dahari [32] analyze heat transfer in a plate-fin heat exchanger and they perform the first calculation of values for the momentum transfer coefficient for the flow between the macro and microphases. Imani and Hooman [34] establish that for conditions analogous to those investigated here the local thermal equilibrium theory is valid for a bidisperse porous medium in that one may employ a single temperature field. The results of these articles are invoked here when we employ the numerical parameter values from Gentile and Straughan [25].

Beavers and Joseph [4] reported values of α for a single-porosity material in the range 0.1–4. These values are for a granular aloxite material and for man-made porous foams. The values of bidisperse parameters reported in Gentile and Straughan [25] suggest that we take relative permeabilities of

$$K_r = 25, 151.7, 263.16$$

and values for the nondimensional momentum transfer coefficient in the group

$$\xi = 1.515 \times 10^{-2}, 2.347 \times 10^{-2}, 2.987 \times 10^{-2}, 0.1316.$$

We here choose to investigate the behavior of the critical Ra_m and a_m values upon $K_r, \alpha^f, \alpha^p\xi$, and we allow $K_r = 10$.

For core values using glass beads and water, the thermal conductivities, densities, and specific heats are taken from the Internet version of Engineering Toolbox to yield $k_m, k_f, (\rho c)_m$, and $(\rho c)_f$. We also employ the parameter ranges in Gentile and Straughan [25] to find values for ξ, K_r, and δ. In this way, we obtain $Pr = 6, Pr_m = 0.75828$, $Da = 0.161278 \times 10^{-2}$, $\delta = 0.3279 \times 10^{-2}$, $\hat{k} = 0.16736$, $\xi = 0.02987$, and $\hat{\kappa} = 0.12638$, although specific values will be varied at appropriate points in our discussion. The nature of the onset of convective motion in all cases depends on $\hat{d}$, the depth of fluid layer to depth of porous layer. There is a critical value of $\hat{d}$ such that when $\hat{d}$ is below this value then convective motion commences in the porous layer whereas such motion is initiated in the fluid layer when $\hat{d}$ is above the critical value. The critical $\hat{d}$ value depends very strongly on the other parameters in the problem and this variation is examined in detail here. This bimodal nature of convection is already known in the two-layer system with a single-porosity medium (see, e.g., Chen and Chen [16]). However, we here highlight differences which we see only in the bidisperse case, especially involving the variation of macro and micro permeability, via K_r, and the variation of

TABLE 1 | The minimum values of the porous Rayleigh number and corresponding wavenumber for the first minimum, Ra_m, a_m, and the second minimum, $Ra_m^{(2)}, a_m^{(2)}$, indicating where instability switches from initiation in the porous layer to the fluid layer. Here, $\delta = 0.003279$, $\hat{k} = 0.16736$, $\xi = 0.02987$, and $\hat{\kappa} = 0.12638$.

Kr	$\hat{d}$	α_p	α_f	a_m	Ra_m	$a_m^{(2)}$	$Ra_m^{(2)}$
10	0.12	0.1	0.3285	2.11	9.83747	18.73	9.84198
10	0.12	0.1	0.3286	2.11	9.84649	18.73	9.84134
15.84	0.12	0.1	0.5	2.39	15.80169	18.37	15.79784
15.85	0.12	0.1	0.5	2.39	15.79928	18.37	15.80973
10	0.1514	0.1	0.3	1.43	3.74989	14.86	3.75241
10	0.1515	0.1	0.3	1.43	3.74305	14.85	3.74187
10	0.0971	0.1	0.65	2.57	21.39214	22.27	21.44558
10	0.0972	0.1	0.65	2.57	21.37669	22.25	21.35607
25	0.1210	0.1	1.25	2.55	21.93729	17.56	21.99490
25	0.1211	0.1	1.25	2.55	21.92427	17.55	21.92237
151.7	0.20	0.1	2	3.0	16.5495	10.0	17.3917
151.7	0.21	0.1	2	3.0	15.5249	10.0	14.3970
151.7	0.1907	0.1	4	2.54	19.44888	10.57	19.47030
151.7	0.1908	0.1	4	2.54	19.43946	10.56	19.43068

the Beavers–Joseph coefficients α^f and α^p, via their ratio, $\alpha^r = \alpha^f/\alpha^p$.

Table 1 displays parameter values for the transition from convection in the porous layer to convection in the fluid layer. The lower of values Ra_m and $Ra_m^{(2)}$ demonstrates where convection commences. When Ra_m is lower, convection initiates in the porous layer, when $Ra_m^{(2)}$ is lower convection initiates in the fluid layer. The first two sets of values in Table 1 show that if we keep $K_r, \alpha_p, \hat{d}$ fixed then changing α^f can change whether convection occurs in the porous layer or in the fluid layer. The second two sets of values in Table 1 keep $\hat{d}, \alpha^f, \alpha^p$ fixed and show that changing K_r can change whether convection occurs in the porous layer or in the fluid layer. The next five sets of parameter values in Table 1 show what values of $\hat{d}$ the convection transition occurs at for a variety of values of K_r, α^p, and α^f. It should be noted from Table 1 that $\hat{d}$ has a large variation from 0.0971 to 0.21 depending on what values the other parameters have.

Figure 1 displays the neutral curves of Ra_m against a_m. The parameters K_r, α^p, and $\hat{d}$ are fixed and $\alpha^f = 0.3$ or 0.35. When $\alpha^f = 0.3$, convection occurs first in the porous layer, whereas when $\alpha^f = 0.35$, convection occurs first in the fluid layer. It is notable that the neutral curves cross, a fact not witnessed in previous articles displaying the neutral curves when $\hat{d}$ is changed. Figure 2 displays the neutral curves of Ra_m against a_m, when the parameters α^p, α^f, and $\hat{d}$ are fixed and $K_r = 14$ or 16. When $K_r = 14$, convection initiates in the fluid layer, whereas when $K_r = 16$, convection initiates in the porous layer. Physically, this is to be expected since when $K_r = 16$, the relative permeability is higher, and so convective motion in the saturated porous layer should be easier. We concentrate on showing the novel effects with the problem under study employing a bidisperse porous material. Of course, keeping other parameters fixed and changing $\hat{d}$ will result in a change from initiation in either the porous or the fluid layer. However, this is known also in the single-porosity case. What is new in the bidisperse case is that changing the ratio of the Beavers–Joseph parameters or the relative permeability can also lead to how convective motion will commence.

Velocity eigenfunctions close to the *transition points* for the situation analogous to that pictured in Figures 1 and 2 are

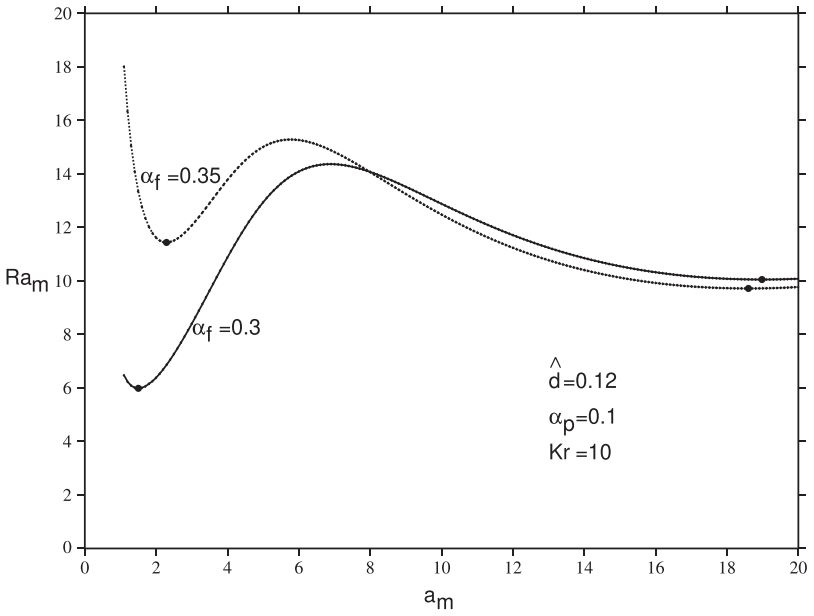

FIGURE 1 | Graph of Ra_m versus a_m. Here, $\delta = 0.003279$, $\hat{k} = 0.16736$, $\alpha_p = 0.1$, $\xi = 0.02987$, $\hat{\kappa} = 0.12638$, $\hat{d} = 0.12$, and $K_r = 10$. The minimum values on the $\alpha_f = 0.3$ curve are at $a_m = 1.50$, $Ra_m = 5.98525$ and $a_m = 18.98$, $Ra_m = 10.05117$, on the $\alpha_f = 0.35$ curve they are $a_m = 2.29$, $Ra_m = 11.43693$ and $a_m = 18.60$, $Ra_m = 9.71738$. The instability when $\alpha_f = 0.3$ initiates in the porous medium, whereas when $\alpha_f = 0.35$, it initiates in the fluid.

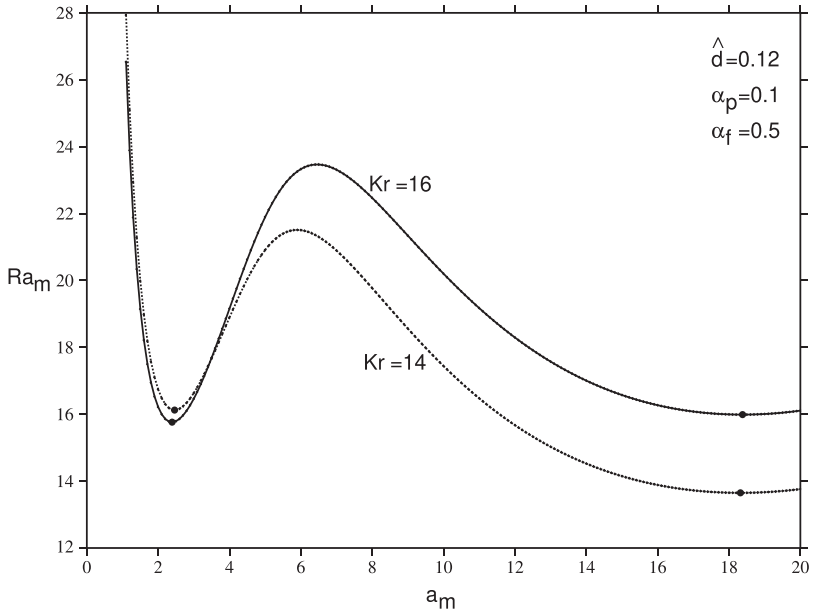

FIGURE 2 | Graph of Ra_m versus a_m. Here, $\delta = 0.003279$, $\hat{k} = 0.16736$, $\hat{d} = 0.12$, $\alpha_p = 0.1$, $\xi = 0.02987$, and $\hat{\kappa} = 0.12638$. The minimum values on the $K_r = 14$ curve are at $a_m = 2.46$, $Ra_m = 16.12391$ and $a_m = 18.32$, $Ra_m = 13.64971$, on the $K_r = 16$ curve they are $a_m = 2.39$, $Ra_m = 13.76240$ and $a_m = 18.38$, $Ra_m = 15.98839$. The instability when $K_r = 16$ initiates in the porous medium, whereas when $K_r = 14$, it initiates in the fluid.

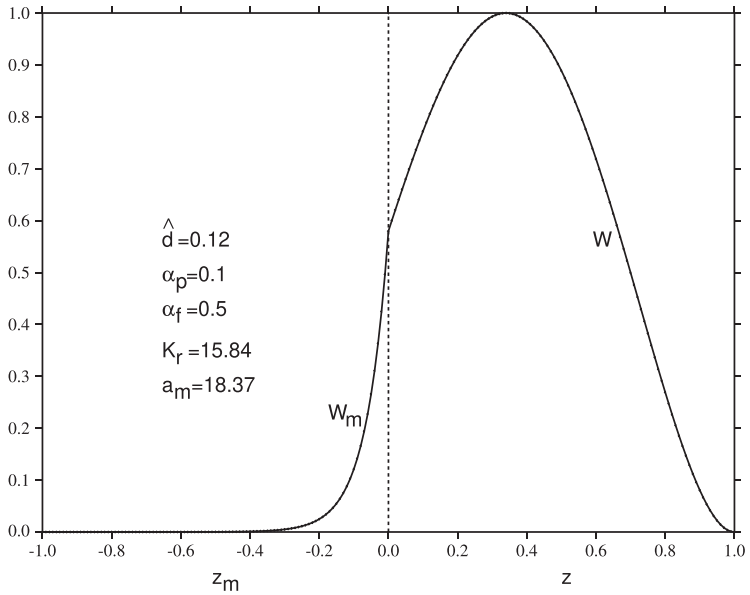

FIGURE 3 | Eigenfunctions for convection initiation in the fluid, W representing the fluid layer with $W_m = W_f + W_p$ representing the porous layer. Here, $a_m = 18.37$, $Ra_m = 15.79784$, other parameters are $K_r = 15.84$, $\delta = 0.003279$, $\hat{k} = 0.16736$, $\hat{d} = 0.12$, $\alpha_p = 0.1$, $\alpha_f = 0.5$, $\xi = 0.02987$, and $\hat{\kappa} = 0.12638$.

displayed in Figures 3, 5, 7, and 9. Figures 4, 6, 8, and 10 show the streamlines corresponding to Figures 3, 5, 7, and 9. The streamlines are not drawn to scale. Since $\hat{d} = 0.12$ the depth of the porous part of the convection cell is 8.33 times larger than that in the fluid. The streamlines are shown only for half a cell since the fluid rises in the center of the cell and descends at the edges. Figure 4 shows that convection is mostly in the fluid region with some movement in the upper part of the porous domain. The half-cell width is $L = \pi/a_m = 0.171018$ and so in Figure 4 the convection cells are relatively narrow and dominated by the fluid. The relative permeability has value 15.84 in this case. However, in Figure 6 the relative permeability is 15.85 and so the fluid can move more freely in the macropores and convection is dominated by the porous layer. For Figure 6, we have $L = \pi/a_m = 1.31447$, and so the half cell in this case is 7.686 times wider than in Figure 4 where the fluid dominates. Even though convection is dominant in the porous layer in Figure 6, the convective motion does extend well into the fluid layer.

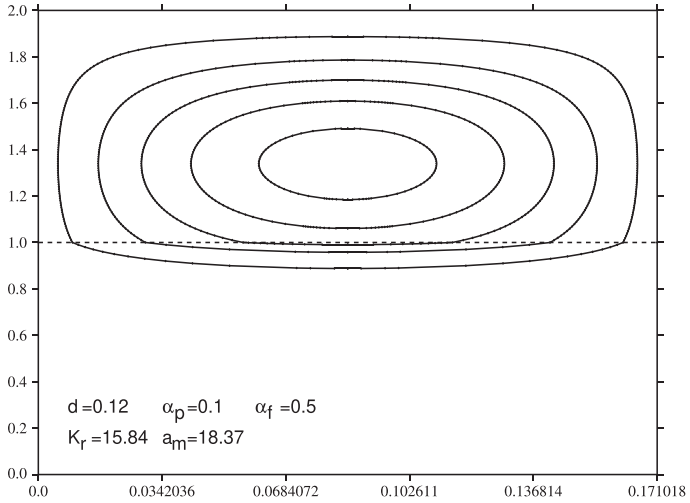

FIGURE 4 | Streamlines for the situation of Figure 3. The inner streamline is for a stream function of value 0.9, then for $\psi = 0.7, 0.5, 0.5$ until the outer streamline has $\psi = 0.1$.

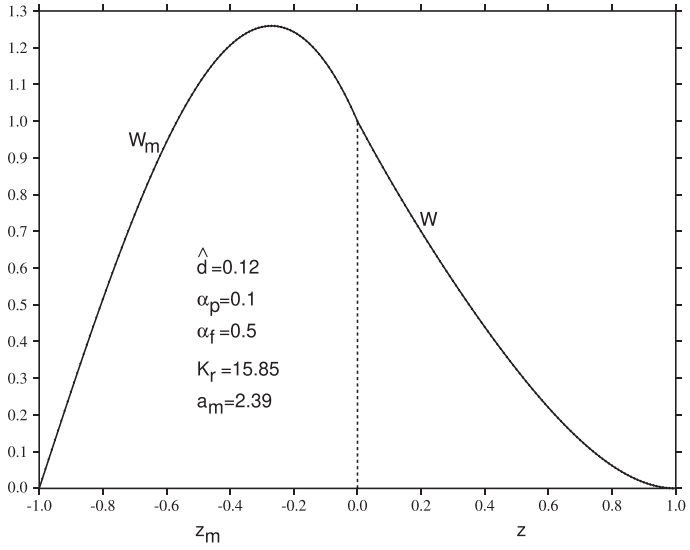

FIGURE 5 | Eigenfunctions for convection initiation in the porous layer, W representing the fluid layer with $W_m = W_f + W_p$ representing the porous layer. Here, $a_m = 2.39$, $Ra_m = 15.79928$, other parameters are $K_r = 15.85$, $\delta = 0.003279$, $\hat{k} = 0.16736$, $\hat{d} = 0.12$, $\alpha_p = 0.1$, $\alpha_f = 0.5$, $\xi = 0.02987$, and $\hat{\kappa} = 0.12638$.

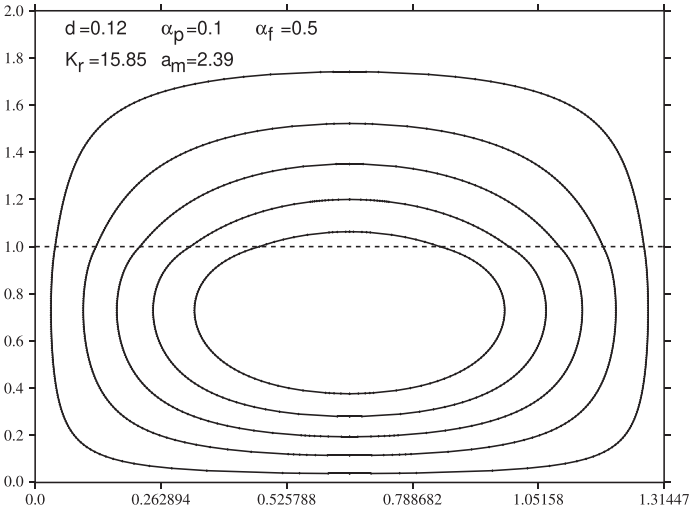

FIGURE 6 | Streamlines for the situation of Figure 5. The inner streamline is for a stream function of value 0.9, then for $\psi = 0.7, 0.5, 0.5$ until the outer streamline has $\psi = 0.1$.

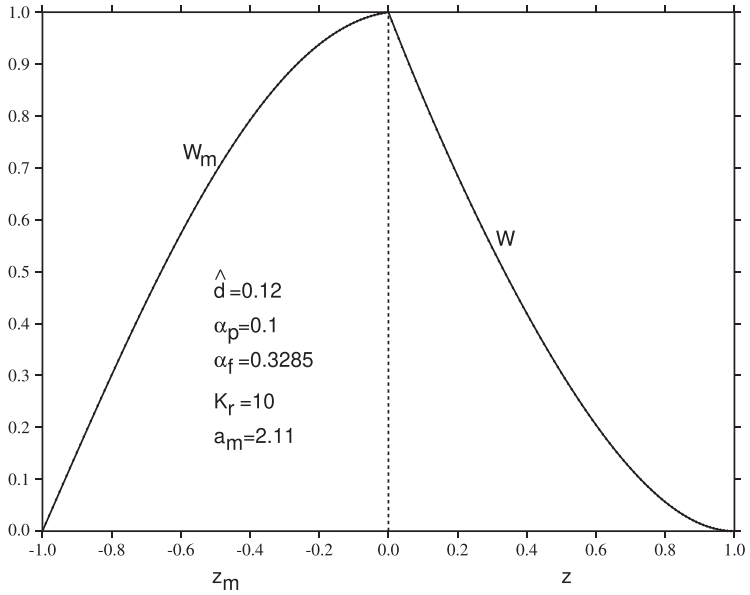

FIGURE 7 | Eigenfunctions for convection initiation in the porous layer, W representing the fluid layer with $W_m = W_f + W_p$ representing the porous layer. Here, $a_m = 2.11$, $Ra_m = 9.83747$, other parameters are $K_r = 10$, $\delta = 0.003279$, $\hat{k} = 0.16736$, $\hat{d} = 0.12$, $\alpha_p = 0.1$, $\alpha_f = 0.3285$, $\xi = 0.02987$, and $\hat{\kappa} = 0.12638$.

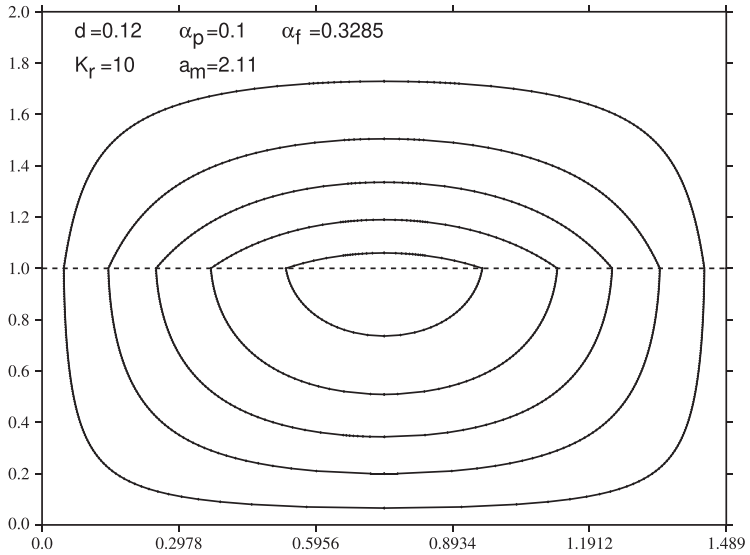

FIGURE 8 | Streamlines for the situation of Figure 7. The inner streamline is for a stream function of value 0.9, then for $\psi = 0.7, 0.5, 0.5$ until the outer streamline has $\psi = 0.1$.

Figures8 and 10 show analogous behavior when the Beavers–Joseph coefficient for the macropores is varied. When $\alpha_f = 0.3285$, the motion in the porous part of the layer is dominant as in Figure 8. However, in Figure 10, $\alpha_f = 0.3286$ and the increase in the Beavers–Joseph coefficient is sufficient to ensure convection is dominated by the fluid layer. The ratio of half-cell widths between Figures 10 and 8 is approximately 8.877.

7 | Conclusions

We have formulated equations for thermal convection in a fluid layer which overlies a layer of bidisperse (or double porosity) porous medium saturated by the same fluid. The macro and micro permeabilities K^f and K^p are explicitly included and play a major role in the model along with the depth of the fluid layer d and the depth of the porous layer d_m. The interface conditions between the fluid and porous medium are very important and we have adopted an approach which assumes continuity of the mass flow rate, but allows for separate Beavers–Joseph conditions appropriate to the macro or micropores. This allows for two Beavers–Joseph interface coefficients α_f and α_p corresponding to the macro and microphases. The permeabilities associated to the macro- and micropores are usually widely different for real porous materials, Gentile and Straughan [25], and using the fundamental results of Beavers and Joseph [4], we analyze

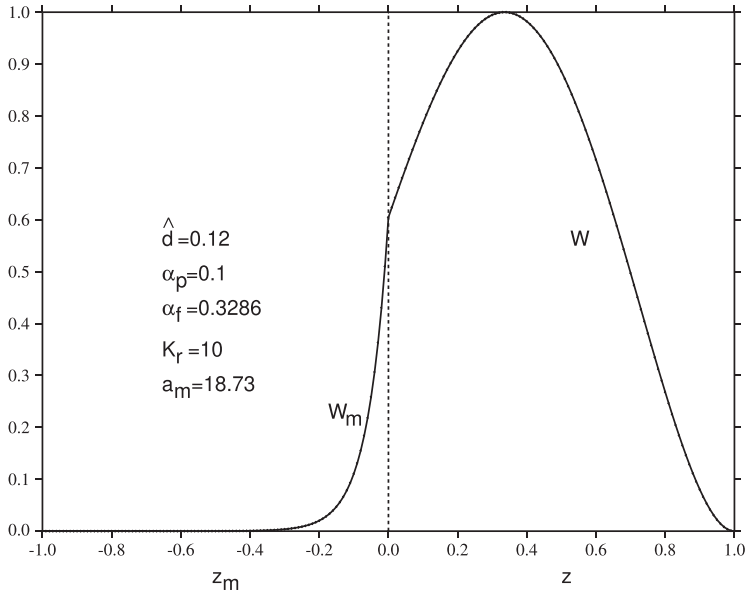

FIGURE 9 | Eigenfunctions for convection initiation in the fluid, W representing the fluid layer with $W_m = W_f + W_p$ representing the porous layer. Here, $a_m = 18.73$, $Ra_m = 9.84134$, other parameters are $K_r = 10$, $\delta = 0.003279$, $\hat{k} = 0.16736$, $\hat{d} = 0.12$, $\alpha_p = 0.1$, $\alpha_f = 0.3286$, $\xi = 0.02987$, and $\hat{\kappa} = 0.12638$.

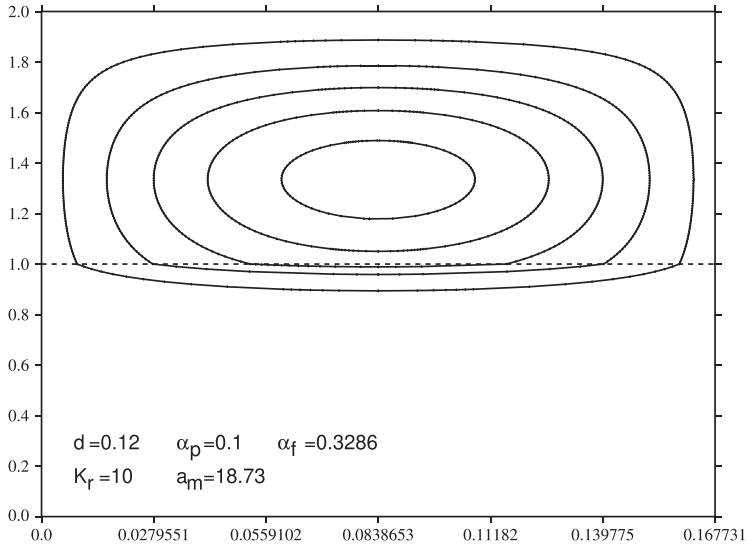

FIGURE 10 | Streamlines for the situation of Figure 9. The inner streamline is for a stream function of value 0.9, then for $\psi = 0.7, 0.5, 0.5$ until the outer streamline has $\psi = 0.1$.

combinations of K_r, α^f, and α^p which may be expected in real life.

Our numerical results show that the bidisperse porous medium is very different from the single porous medium case in that the coefficients of the double porosity material must be taken into account to fully describe thermal convection instability. Since the two-layer convection problem with a fluid overlying a bidisperse porous medium does have serious application to renewable energy generation (see, e.g., Wang et al. [66], Wang, Zhang, and Mei [67]), we believe the current work is very useful. Of course, two-layer convection with a single-porosity medium already has many parameters (see, e.g., Chen [15], Chen and Chen [16–18], Straughan [56, 57]), while convection in a single bidisperse layer likewise involves many parameters. The combined problem is necessarily complicated and, therefore, involves a lot of parameters. Future work will apply this theory to specific renewable energy situations.

Nomenclature

V_i	Fluid velocity
U_i^f	Pore averaged velocity in the macropores
U_i^p	Pore averaged velocity in the micropores

p	Pressure in the fluid
p^f	Fluid pressure in the macropores
p^p	Fluid pressure in the micropores
T	Temperature of the fluid
T^m	Temperature of the fluid in the porous medium
T_U	Temperature of the upper boundary
T_L	Temperature of the lower boundary
ϕ	Porosity associated with the macropores
ϵ	Porosity associated with the micropores
ν	Kinematic viscosity of the fluid
K^f	Permeability associated with the macropores
K^p	Permeability associated with the micropores
k^f	Thermal conductivity of the fluid
$(\rho_0 c_p)_f$	Product of the density and specific heat at constant pressure of the fluid
γ	Thermal expansion coefficient of the fluid
ζ	Coefficient of momentum transfer between the macro and microphases
g	Gravity coefficient
$(\rho_0 c)_m$	Product of the density and specific heat at constant pressure suitably averaged over the porous medium
k_m	Thermal conductivity suitably averaged over the porous medium
k_s	Thermal conductivity of the solid skeleton
μ	Dynamic viscosity of the fluid
ξ	Nondimensional version of the momentum transfer coefficient
Ra	Rayleigh number
Ra_m	Porous Rayleigh number
Pr	Prandtl number
Pr_m	Porous Prandtl number
$\hat{k}$	Ratio of k_f to k_m
$\hat{\kappa}$	Product of $\hat{k}$ and ratio of $(\rho_0 c)_m$ to $(\rho_0 c)_f$
d	Depth of fluid layer
d_m	Depth of the bidisperse porous layer
$\hat{d}$	Ratio of d to d_m
α^f	Beavers–Joseph interface coefficient for the macropores
α^p	Beavers–Joseph interface coefficient for the micropores
K_r	Ratio of K^f to K^p
Da	Darcy number
a	Fluid wavenumber
a_m	Porous wavenumber

Acknowledgments

Open access funding enabled and organized by Projekt DEAL.

Conflicts of Interest

The authors declare no conflicts of interest.

Data Availability Statement

The numerical code used for this manuscript is not made publicly available. Enquiries regarding the method can be made to the corresponding author.

References

1. A. A. Khan and P. Bera, "Stability of Non-Isothermal Poiseuille Flow in a Fluid Overlying an Anisotropic and Inhomogenous Porous Domain," *Journal of Fluid Mechanics* 949 (2022): A44.

2. A. J. Badday and A. J. Harfash, "Chemical Reaction Effect on Convection in Bidispersive Porous Medium," *Transport in Porous Media* 137 (2021): 381–397.

3. N. Barman, A. Aleria, and P. Bera, "Non-Isothermal Plane Couette Flow and Its Stability in an Anisotropic and Inhomogeneous Porous Layer Underlying a Fluid Layer Saturated by Water," *International Journal of Heat and Mass Transfer* 146 (2024):072701.

4. G. S. Beavers and D. D. Joseph, "Boundary Conditions at a Naturally Permeable Wall," *Journal of Fluid Mechanics* 30 (1967): 197–207.

5. F. Capone and R. De Luca, "The Effect of the Vadasz Number on the Onset of Thermal Convection in Rotating Bidispersive Porous Media," *Fluids* 5 (2020):5040173.

6. F. Capone and G. Massa, "The Effects of Vadasz Term, Anisotropy and Rotation on Bi-Disperse Convection," *International Journal of Non-Linear Mechanics* 135 (2021): 103749.

7. F. Capone, R. De Luca, and M. Gentile, "Thermal Convection in Rotating Anisotropic Porous Layers," *Mechanics Research Communications* 110 (2020):103601.

8. F. Capone, R. De Luca, and M. Gentile, "Coriolis Effect on Thermal Convection in a Rotating Bidispersive Porous Layer," *Proceedings of the Royal Society of London. Series A* 476, no. 2235 (2020): 1–8.

9. F. Capone, R. De Luca, and G. Massa, "Effect of Anisotropy on the Onset of Convection in Rotating Bi-Disperse Brinkman Porous Media," *Acta Mechanica* 232 (2021): 3393–3406.

10. M. Carr and B. Straughan, "Penetrative Convection in a Fluid Overlying a Porous Layer," *Advances in Water Resources* 26 (2003): 263–276.

11. H. A. Chaloob, A. J. Harfash, and A. J. Harfash, "Bidispersive Thermal Convection With Relatively Large Macropores and Generalized Velocity and Temperature Boundary Conditions," *Physics of Fluids* 33 (2021):014105.

12. S. Chandrasekhar, *Hydrodynamic and Hydromagnetic Stability* (New York: Dover, 1981).

13. M. H. Chang, F. Chen, and B. Straughan, "Instability of Poiseuille Flow in a Fluid Overlying a Porous Layer," *Journal of Fluid Mechanics* 564 (2006): 287–303.

14. T. Y. Chang, F. Chen, and M. H. Chang, "Stability of Plane Poiseuille–Couette Flow in a Fluid Layer Overlying a Porous Layer," *Journal of Fluid Mechanics* 826 (2017): 376–395.

15. F. Chen, "Throughflow Effects on Convective Instability in Superposed Fluid and Porous Layers," *Journal of Fluid Mechanics* 231 (1991): 113–133.

16. F. Chen and C. F. Chen, "Onset of Finger Convection in a Horizontal Porous Layer Underlying a Fluid Layer," *Journal of Heat Transfer* 110 (1988): 403–409.

17. F. Chen and C. F. Chen, "Experimental Investigation of Convective Stability in a Superposed Fluid and Porous Layer When Heated From Below," *Journal of Fluid Mechanics* 207 (1989): 311–321.

18. F. Chen and C. F. Chen, "Convection in Superposed Fluid and Porous Layers," *Journal of Fluid Mechanics* 234 (1992): 97–119.

19. J. J. Dongarra, B. Straughan, and D. W. Walker, "Chebyshev Tau-QZ Algorithm Methods for Calculating Spectra of Hydrodynamic Stability Problems," *Applied Numerical Mathematics* 22 (1996): 399–435.

20. M. Ehrhardt, *An Introduction to Fluid-Porous Interface Coupling* (Technical report, Bergische Universität Wuppertal, 2010). Preprint BUW-AMNA-OPAP 10/15.

21. P. Falsaperla, G. Mulone, and B. Straughan, "Bidispersive Inclined Convection," *Proceedings of the Royal Society of London. Series A* 472 (2016):20160480.

22. F. Franchi, R. Nibbi, and B. Straughan, "Continuous Dependence on Modelling for Temperature Dependent Bidispersive Flow," *Proceedings of the Royal Society of London. Series A* 473 (2017):20170485.

23. M. Gentile and B. Straughan, "Bidispersive Thermal Convection," *International Journal of Heat and Mass Transfer* 114 (2017): 837–840.

24. M. Gentile and B. Straughan, "Bidispersive Vertical Convection," *Proceedings of the Royal Society A* 473 (2017):20170481.

25. M. Gentile and B. Straughan, "Bidispersive Thermal Convection With Relatively Large Macropores," *Journal of Fluid Mechanics* 898 (2020): A14.

26. D. Z. Han, Q. Wang, and X. M. Wang, "Dynamic Transitions and Bifurcations for Thermal Convection in the Superposed Free Flow and Porous Media," *Physica D* 414 (2020):132687.

27. Y. Hibi, "Modeling Variable Density Flow in Subsurface and Surface Water in the Vicinity of the Boundary Between a Surface Water-Atmosphere System and the Subsurface," *Journal of Contaminant Hydrology* 234 (2020):103688.

28. Y. Hibi and A. Tomigashi, "Evaluation of a Coupled Model for Numerical Simulation of a Multiphase Flow System in a Porous Medium and a Surface Fluid," *Journal of Contaminant Hydrology* 180 (2015): 34–55.

29. A. A. Hill and B. Straughan, "Poiseuille Flow of a Fluid Layer Overlying a Porous Layer," *Journal of Fluid Mechanics* 603 (2008): 137–149.

30. A. A. Hill and B. Straughan, "Global Stability for Thermal Convection in a Fluid Overlying a Highly Porous Material," *Proceedings of the Royal Society of London. Series A* 465 (2009): 207–217.

31. A. A. Hill and B. Straughan, "Poiseuille Flow in a Fluid Overlying a Highly Porous Material," *Advances in Water Resources* 32 (2009): 1609–1614.

32. K. Hooman, E. Sauret, and M. Dahari, "Theoretical Modelling of Momentum Transfer Function of Bi-Disperse Porous Media," *Applied Thermal Engineering* 75 (2015): 867–870.

33. S. Hooshyar, H. N. Yoshikawa, and P. Mirbod, "The Impact of Imposed Couette Flow on the Stability of Pressure-Driven Flows Over Porous Surfaces," *Journal of Engineering Mathematics* 132 (2022): 15.

34. G. Imani and K. Hooman, "Lattice Boltzmann Pore Scale Simulation of Natural Convection in a Differentially Heated Enclosure Filled With a Detached or Attached Bidisperse Porous Medium," *Transport in Porous Media* 116 (2017): 91–113.

35. S. Kumaravel, M. Nagaraj, and P. Barmavatu, "Experimental and Theoretical Investigation to Optimize the Performance of Solar Still," *Desalination and Water Treatment* 318 (2024): 100343, https://doi.org/10.1016/j.dwt.2024.100343.

36. Y. Li, S. Xiao, and Y. Lin, "Continuous Dependence for the Brinkman-Forchheimer Fluid Interacting With a Darcy Fluid in a Bounded Domain," *Mathematics and Computers in Simulation* 150 (2018): 66–82.

37. Y. Li, X. Chen, and J. Shi, "Structural Stability in Resonant Penetrative Convection in a Brinkman-Forchheimer Fluid Interfacing With a Darcy Fluid," *Applied Mathematics and Optimization* 84 (2021): 979–999.

38. Y. Li, S. Zhang, and C. Lin, "Structural Stability for the Boussinesq Equations Interfacing With Darcy Equations in a Bounded Domain," *Boundary Value Problems* 2021 (2021), https://doi.org/10.1186/s13661-021-01501-0.

39. W. Q. Lyu and X. M. Wang, "Stokes-Darcy System, Small Darcy Number Behaviour and Related Interfacial Conditions," *Journal of Fluid Mechanics* 922 (2021): A4.

40. M. McCurdy, M. N. Moore, and X. Wang, "Convection in a Coupled Free Flow-Porous Media System," *SIAM Journal on Applied Mathematics* 79 (2019): 2313–2338.

41. G. McKay and B. Straughan, "Patterned Ground Formation Under Water," *Continuum Mechanics and Thermodynamics* 5 (1993): 145–162.

42. P. Mirbod, S. Hooshyar, E. Taheri, and H. N. Yoshikawa, "On the Instability of Particle-Laden Flows in Channels With Porous Walls," *Physics of Fluids* 36 (2024):044105.

43. C. B. Moler and G. W. Stewart, *An Algorithm for the Generalized Matrix Eigenvalue Problem* $Ax = \lambda Bx$ (Technical report, Univ. Texas at Austin, 1971).

44. D. A. Nield, "Onset of Convection in a Fluid Layer Overlying a Layer of Porous Medium," *Journal of Fluid Mechanics* 81 (1977): 513–522.

45. D. A. Nield, "Modelling Fluid Flow and Heat Transfer in a Saturated Porous Medium," *Journal of Applied Mathematics & Decision Sciences* 81 (1977): 165–173.

46. D. A. Nield and A. V. Kuznetsov, "The Onset of Convection in a Bidisperse of Porous Medium," *International Journal of Heat and Mass Transfer* 49 (2006): 3068–3074.

47. L. E. Payne and B. Straughan, "Analysis of the Boundary Condition at the Interface Between a Viscous Fluid and a Porous Medium and Related Modelling Questions," *Journal de Mathématiques Pures et Appliquées* 77 (1998): 317–354.

48. R. Ponalagusamy and R. Manchi, "Mathematical Study on Two-Fluid Model for Flow of K-L Fluid in a Stenosed Artery With Porous Wall," *SN Applied Sciences* 3 (2021): 508.

49. D. A. S. Rees, "Microscopic Modelling of the Two-Temperature Model for Conduction in Heterogeneous Media: Three-Dimensional Media," in *Proceedings of the Fourth International Conference on Applications of Porous Media*, Vol. 13 (Istanbul: ICAPM, 2009), 125–143.

50. D. A. S. Rees, "Microscopic Modelling of the Two-Temperature Model for Conduction in Heterogeneous Media," *Journal of Porous Materials* 13 (2010): 125–143.

51. A. Samanta, "Linear Stability of a Plane Couette-Poiseuille Flow Overlying a Porous Layer," *International Journal of Multiphase Flow* 123 (2020):103160.

52. A. Samanta, "Nonmodal and Modal Analyses of Flow Through Inhomogeneous and Anisotropic Porous Channel," *International Journal of Multiphase Flow* 157 (2022):104230.

53. A. Samanta, "Modal Analysis of a Fluid Flowing Over a Substrate," *Theoretical and Computational Fluid Dynamics* 37 (2023): 241–260.

54. S. Saravanan and S. Vigneshwaran, "Centrifugal Filtration Convection in Bidisperse Media," *Physics of Fluids* 32 (2020):084109.

55. B. D. Sharma and P. K. Yadav, "A Two-Layer Mathematical Model of Blood Flow in Porous Constricted Blood Vessels," *Transport in Porous Media* 120 (2017): 239–254.

56. B. Straughan, "Surface-Tension-Driven Convection in a Fluid Overlying a Porous Layer," *Journal of Computational Physics* 170 (2001): 320–337.

57. B. Straughan, "Effect of Property Variation and Modelling on Convection in a Fluid Overlying a Porous Layer," *International Journal for Numerical and Analytical Methods in Geomechanics* 26 (2002): 75–97.

58. B. Straughan, *Stability, and Wave Motion in Porous Media*, Vol. 165, Appl. Math. Sci. (New York: Springer, 2008).

59. B. Straughan, *Mathematical Aspects of Multi-Porosity Continua*, Vol. 38, Advances in Mechanics and Mathematics Series (Cham, Switzerland: Springer, 2017).

60. B. Straughan, "Horizontally Isotropic Bidispersive Thermal Convection," *Proceedings of the Royal Society of London. Series A* 474 (2018):20180018.

61. B. Straughan, "Anisotropic Bidispersive Convection," *Proceedings of the Royal Society of London. Series A* 475 (2019):20190206.

62. B. Straughan, "Horizontally Isotropic Double Porosity Convection," *Proceedings of the Royal Society of London. Series A* 475 (2019):20180672.

63. A. Tiwari, P. D. Shah, and S. S. Chauhan, "Solute Dispersion in Two-Fluid Flowing Through Porous Tubes With a Porous Layer Near the Absorbing Wall: Model for Dispersion Phenomenon in Microvessels," *International Journal of Multiphase Flow* 131 (2020):103380.

64. K. Tsiberkin, "Porosity Effect on the Linear Stability of Flow Overlying a Porous Medium," *European Physical Journal* 43 (2020): 34.

65. S. A. Wajihah and D. S. Sankar, "Effects of Porosity in Four-Layared Nonlinear Blood Rheology in Constricted Narrow Arteries With Clinical Applications," *Computer Methods and Programs in Biomedicine* 199 (2021):105907.

66. H. Wang, X. L. Yu, F. Shen, and L. Zhang, "A Laboratory Experimental Study on Effect of Porous Medium on Salt Diffusion of Salt Gradient Solar Pond," *Solar Energy* 122 (2015): 630–639.

67. H. Wang, L. G. Zhang, and Y. Y. Mei, "Investigation on the Exergy Performance of Salt Gradient Solar Ponds With Porous Media," *International Journal of Exergy* 25 (2018): 34–53.

68. Z. Wu and P. Mirbod, "Instability Analysis of the Flow Between Two Parallel Plates Where the Bottom One is Coated With Porous Media," *Advances in Water Resources* 130 (2019): 221–228.

69. C. Yin, C. W. Wang, and S. W. Wang, "Thermal Instability of a Viscoelastic Fluid in a Fluid-Porous System With a Plane Poiseuille Flow," *Applied Mathematics and Mechanics* 41 (2020): 1631–1650.